



# Mechano-Plastic Pyrolysis of Dynamic Covalent Polymer Network toward Hierarchical 3D Ceramics

Ning Zheng, Jingjing Hou, Hangbo Zhao, Jingjun Wu, Yingwu Luo, Hao Bai, John A. Rogers, Qian Zhao,\* and Tao Xie\*

Shaping ceramics into complex 3D geometries is desirable yet challenging, particularly those with structural hierarchy spanning different length scales. A mechano-plastic pyrolysis process that overcomes this limitation is reported. In addition to taking advantage of the moldability of organic polymers, the process uniquely incorporates mechano-plasticity via dynamic covalent bond exchange for reconfiguring the shape of a preceramic polymer. The combined steps result in simultaneous shape control at both micro- and macro-scales. Further pyrolysis leads to complex ceramic structures that are otherwise difficult to produce. To enable this process, rational design of the polymer network is required to satisfy an unusual combination of mechano-plasticity and pyrolysis. Overall, the process offers an avenue for efficient fabrication of hierarchical 3D ceramic structures suitable for engineering applications.

The high temperature resistance of ceramics makes them uniquely suited for many applications in which, typical metals and organic polymers often fail. Their intrinsic brittle nature, however, severely limits the options for processing. For instance, they cannot be machined as easily as metals and polymers. Producing ceramics with intricate geometric features spanning both the macroscopic and microscopic scales is particularly challenging, in contrast to the ever-increasing demand for high-value added applications.<sup>[1–4]</sup> Casting that

employs ceramic powder, along with other additives (e.g., binder), represents the most common technique for ceramic processing.<sup>[5,6]</sup> Complex macroscopic 3D parts can be produced via sacrificial molding. However, simultaneous structural control at the microscopic scale is difficult due to the size of the powder and the equally difficult fabrication of the corresponding hierarchical mold. Preceramic approach takes advantage of the easy processability of preceramic organic polymers.<sup>[7–9]</sup> Pyrolysis after the polymer micromolding leads to ceramics with microscopic features suitable for various applications including microgears for microelectromechanical systems,<sup>[2]</sup> high temperature photonic crystals,<sup>[3]</sup> and wire guides

in textile manufacturing.<sup>[4]</sup> The planar nature of the micromolds as intrinsically limited by typical lithographic methods used to produce them means that simultaneous control of the 3D geometry at the macroscopic level is not feasible.<sup>[2,10]</sup> 3D printing offers an alternative option to produce macroscopic 3D ceramics in a highly versatile manner without the limitation of molds.<sup>[11,12]</sup> Unfortunately, its resolution is typically limited to tens of micrometers, making it unsuitable for applications that requires microstructure precision. In theory, finer resolution in the submicron range can be achieved by employing two-photon techniques.<sup>[13,14]</sup> This, however, comes at the cost of losing entirely the macroscopic productivity. Self-shaping ceramics relies on the stress from the aligned platelet precursors<sup>[15]</sup> or preceramic assemblies<sup>[16]</sup> to produce 3D shapes. Although it forgoes the need for mold, the method cannot achieve control at the small scale. In contrast to the above shortcomings, we describe herein a new ceramics processing technique that allows simultaneous control of the geometric features at the macroscopic and microscopic scales.

The principle of our method, called mechano-plastic pyrolysis (MPP), is schematized in **Figure 1a**. The process consists of a mechano-plastic shaping step and a subsequent pyrolysis step. We start from a 2D flat butterfly-shape preceramic polymer (poly(dimethylsiloxane) (PDMS)) film with a (sub)micron surface pattern obtained by conventional liquid micromolding. The micromolding method confines its macroscopic shape to two dimensions due to the intrinsic limitation of the lithographic technique used to create the silicon micromold. Herein, the colors indicate that the surface feature size approaches the wavelength of visible light, causing

N. Zheng, J. Hou, Dr. J. Wu, Prof. Y. Luo, Prof. H. Bai, Prof. Q. Zhao, Prof. T. Xie  
State Key Laboratory of Chemical Engineering  
College of Chemical and Biological Engineering  
Zhejiang University  
38 Zheda Road, Hangzhou 310027, P. R. China  
E-mail: qianzhao@zju.edu.cn; taoxie@zju.edu.cn

Dr. H. Zhao, Prof. J. A. Rogers  
Center for Bio-Integrated Electronics  
Northwestern University  
Evanston, IL 60208, USA

Prof. J. A. Rogers  
Department of Materials Science and Engineering  
Biomedical Engineering, Chemistry  
Mechanical Engineering  
Electrical Engineering, and Computer Science  
Neurological Surgery  
Simpson Querrey Institute and Feinberg Medical School  
Northwestern University  
Evanston, IL 60208, USA

DOI: 10.1002/adma.201807326

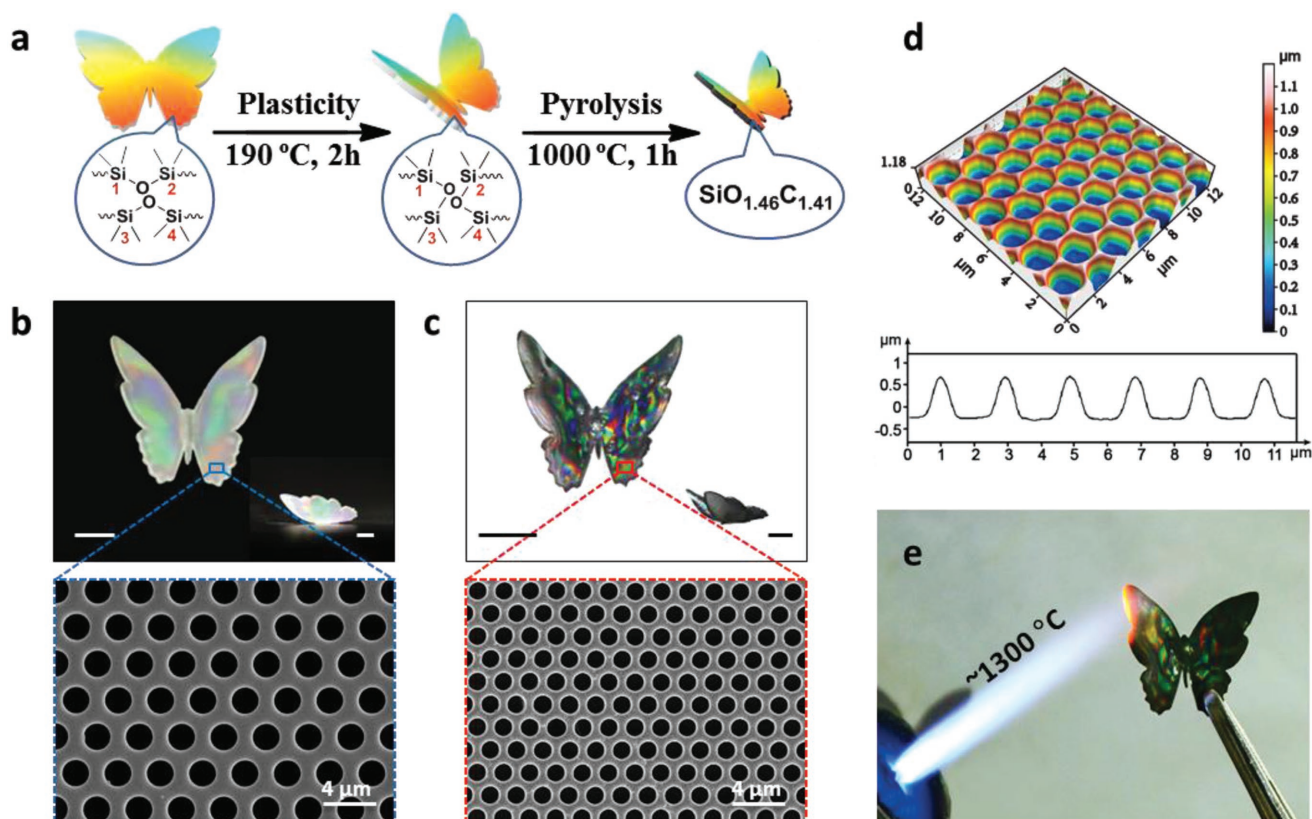


**Figure 1.** Mechano-plastic pyrolysis (MPP) for making hierarchical ceramics. a) Schematic illustration of the plastic deformation and pyrolysis. b) Macroscopic photographic image (scale bar: 1 cm; insert: side view) and SEM image of the 3D preceramic PDMS. c) Macroscopic photographic image (scale bar: 1 cm; insert: side view) and SEM image of the 3D ceramics. d) Confocal laser scanning microscopic image of surface microstructures on the ceramics. e) Demonstration of high temperature shape stability of the resultant ceramics.

interference. Of critical importance to the MPP process is that the siloxane bonds of PDMS can be thermally triggered for dynamic bond exchange. This leads to the so-called plasticity<sup>[17–22]</sup> that allows permanently deforming the material, opposite to the commonly known rubber elasticity for PDMS. Accordingly, the structurally colored 2D butterfly is deformed permanently into a macroscopic 3D shape at 190 °C, a temperature sufficiently high to trigger plasticity. Critically, the microscopic surface pattern is well preserved during the plastic deformation. Upon further pyrolysis by programmed heating to 1000 °C at the rate of 1 °C min<sup>-1</sup>, the PDMS is converted into the corresponding macroscopic 3D ceramics (SiOC) with the surface micropattern. Figure 1b shows that the actual PDMS butterfly produced, with the photographic top and side views demonstrating its macroscopic 3D shape and the structural colors. The scanning electron microscopy (SEM) image confirms the microscopic surface pattern with feature size around 2 μm. Importantly, upon pyrolysis the colors and the macroscopic and microscopic geometric features are carried onto the ceramics (Figure 1c), with the linear shrinkage of 53.5%. The surface feature depth is about 0.94 μm (Figure 1d). Elementary analysis suggests that the resultant ceramic is SiO<sub>1.46</sub>C<sub>1.41</sub>. The 3D structurally colored butterfly shows excellent high temperature shape stability (Figure 1e), further confirming its ceramic nature.

While seemingly simple and straightforward, two key points enabling the MPP are noteworthy. First, the covalent bond exchange mechanism behind the plasticity has been demonstrated for various dynamic chemistries including transesterification,<sup>[17,18]</sup> transcarbamoylation,<sup>[19]</sup> TAD chemistry,<sup>[20]</sup> Diels–Alder reaction,<sup>[21]</sup> addition–fragmentation chain transfer reaction,<sup>[22]</sup> and disulfide bond exchange.<sup>[23]</sup> Typically, the mechanism is utilized for recycling of thermoset polymers via melting.<sup>[24–26]</sup> Intriguingly, our results shown in Figure 1 suggest no sign of melting throughout the entire process, otherwise the microscopic feature would either disappear entirely or at minimum be severely compromised. Second, even though siloxane equilibration triggered by anionic species<sup>[27,28]</sup> has been documented for self-healing and remolding of PDMS, enabling the MPP process requires adjusting the chemistry from a completely different perspective.

Specifically, we use commercial Sylgard 184 (curing agent/base = 1/10, platinum-based catalyst) as the base PDMS network (Figure 2a). While the platinum-based catalyst ensures the PDMS curing (crosslinking), an additional base catalyst (sodium octanoate) is introduced in the formulation as the active species for inducing the bond exchange. This system is chosen by carefully considering various scenarios that can occur in the MPP process. First, the bond exchange (Figure 2b)

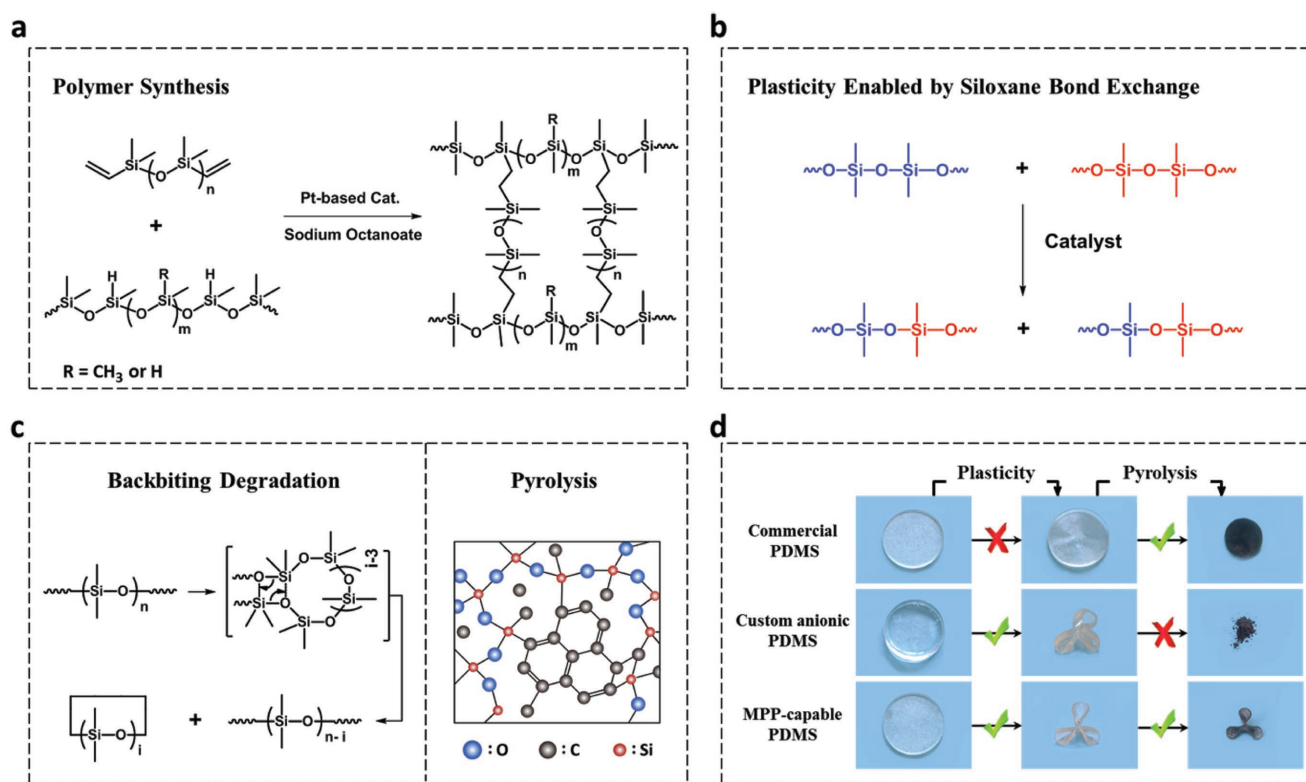


**Figure 2.** Chemical design of MPP-capable PDMS. a) MPP-capable PDMS network. ( $n \approx 60$ ,  $m \approx 10$ ) b) Siloxane bond exchange chemistry during the plasticity process. c) Backbiting degradation mechanism during pyrolysis and ceramic network structure after pyrolysis. d) Comparison of plasticity and pyrolysis of various PDMS.

should be activated to enable the plasticity. During subsequent high temperature pyrolysis, the network may undergo degradation via chain unzipping to produce small molecular byproducts (Figure 2c). This degradation should be properly controlled in order to enable the pyrolysis that results in the desired ceramic product. Meeting these different, seemingly contradictory, requirements is not straightforward. Figure 2d shows that commercial PDMS without sodium octanoate as the catalyst does not possess the plasticity although it can be successfully pyrolyzed with ceramic yield of 37.4%. On the contrary, a custom synthesized PDMS via anion polymerization catalyzed by tetramethylammonium hydroxide<sup>[27]</sup> shows excellent plasticity, but pyrolysis leads to a powdery product with a low ceramic yield (2.9%) and a significant amount of oily residues due to the undesirable degradation. We decide to focus on commercial PDMS as the matrix and screen various base catalysts to induce the plasticity (Table S1, Supporting Information). Many base catalysts favor plasticity but are disadvantageous for the pyrolysis process. Sodium octanoate (used hereafter) is selected as a compromise solution based on its optimum performance in terms of its solubility and balancing the plasticity and pyrolysis (with a ceramic yield of 17.3%).

Various parameters can impact the plasticity, which is characterized in iso-strain–stress relaxation experiments. More catalyst favors faster relaxation (Figure S1, Supporting Information) and lower residual stress (Figure 3a). At the low concentration range, more catalyst leads to drastic reduction

of ceramic yield/linear shrinkage upon pyrolysis (Figure 3b), but such a reduction reaches plateau values (ceramic yield of 17.3% and linear shrinkage of 53.5%) at 0.03% of catalyst. A catalyst amount of 0.1% was thus chosen for the remaining experiments due to its balanced performance in terms of plasticity and ceramic yield upon pyrolysis. Under this condition, higher temperature promotes faster stress relaxation and lower residual stress (Figure 3c), corresponding to an activation energy of  $119.3 \text{ kJ mol}^{-1}$ . The stress relaxation kinetics is consistent with the theoretical prediction by a stretched exponential function model (see Methods and Table S2 in the Supporting Information).<sup>[29,30]</sup> The stress relaxation is also affected by the constant strain imposed in the experiments, with a larger strain resulting in faster relaxation kinetics (Figure S2, Supporting Information). Figure 3d illustrates the cumulative nature of the plasticity in consecutive cycles of partial relaxation experiments. In each cycle, a sample is first stretched to a constant strain of 50% and the stress is partially relaxed. Upon removal of the residual external stress, the sample is allowed to reach its equilibrium length prior to the next cycle. The fact that stress can be relaxed upon consecutive cycling suggests that multiple permanent shape reconfigurations can be imposed and accumulated in the same sample. This is visually demonstrated in the inset in Figure 3d. A first set of parallel strips are permanently embossed onto an original featureless sample (Figure S3, Supporting Information). A second set of strips perpendicular to the first set can be further imprinted, importantly without

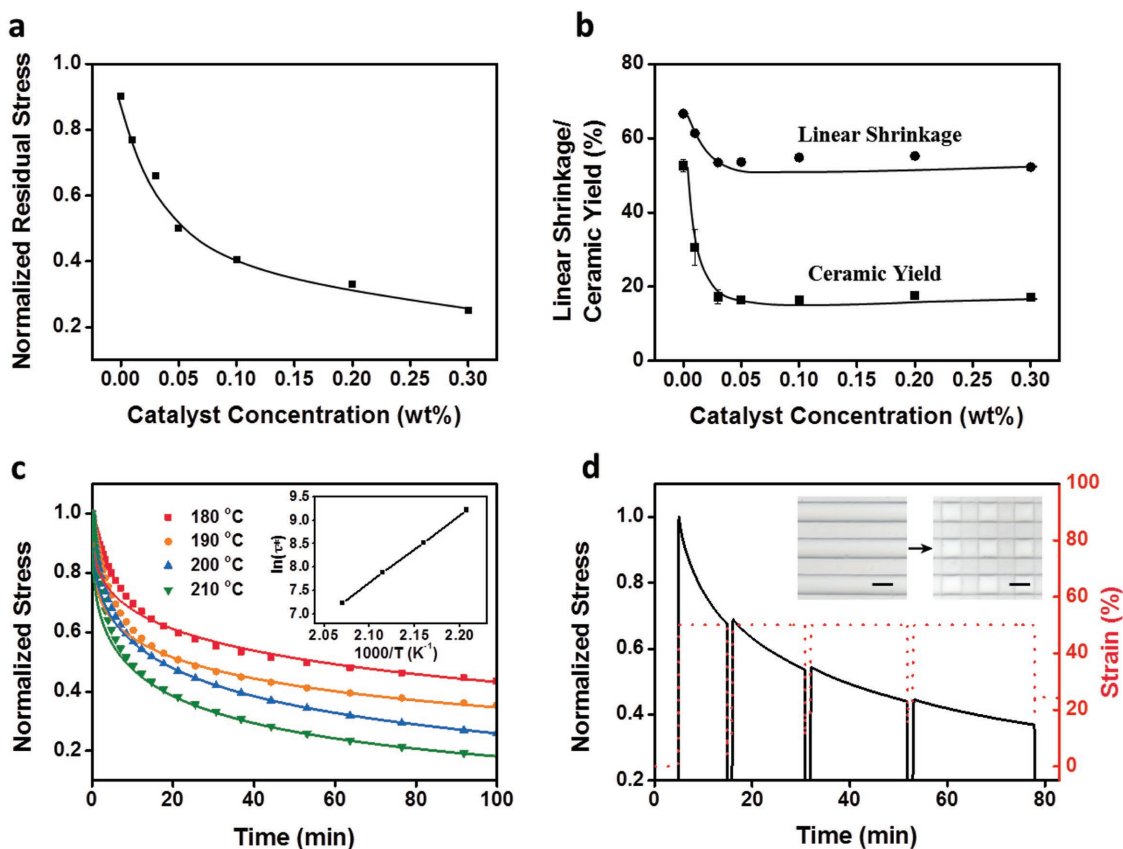


**Figure 3.** Quantitative evaluation of plasticity and the ability of pyrolysis. a) Normalized residual stress for various catalyst (sodium octanoate) concentrations (isostrain: 50%, 190 °C, 100 min). b) Linear shrinkage and ceramic yield after pyrolysis. c) Iso-strain–stress relaxation at various temperatures and the corresponding Arrhenius analysis (0.1% catalyst, 50% strain), solid lines represents theoretical fitting results (Table S2, Supporting Information). d) Consecutive four partial stress cycles at 190 °C. Insert: optical images illustrating shape accumulation (scale bar: 50  $\mu\text{m}$ ).

deleting the first one. This cumulative effect can be uniquely beneficial for making complex structures.

The MPP process opens up ample opportunities for making ceramics of complex geometries. **Figure 4a–c** shows that flat laser cut PDMS sheets can be deformed permanently via plasticity into various 3D shapes, which upon pyrolysis result in the corresponding ceramics. The bond exchangeability within the PDMS network also leads to an unusual opportunity to assemble 3D structures by bonding various PDMS samples of different shapes via interfacial bond exchange (i.e., self-bonding). **Figure 4d** demonstrates that the resulting multilayer PDMS structure can be successfully converted into ceramics. The MPP process can be readily extended to PDMS composites with various inorganic nanoparticles as the fillers (**Figure S4**, Supporting Information). **Figure 4e** illustrates another notable flexibility of the MPP process. A microstructured PDMS can be repeatedly manipulated via molding, plasticity, and pyrolysis. With the plasticity altering the feature shape and pyrolysis reducing the feature size, a variety of microstructures can be obtained using the same starting PDMS. We emphasize that a key distinction to other dynamic covalent networks<sup>[24–26]</sup> is that no material flow occurs during the plastic deformation of PDMS (**Figure S5**, Supporting Information), otherwise the microstructures would be erased

or distorted during the process. The unique features of the MPP process can be further explored for making functional ceramic devices. Using laser engraving and interfacial self-bonding, a PDMS with an embedded microchannel was created (**Figure 4f**). Following the MPP, a snake-shaped ceramic microfluidic device was fabricated (**Figure 4g**). With the thermal conductivity of  $1.207 \text{ W m}^{-1} \text{ K}^{-1}$ , this ceramic heat radiator shows performance superior to that of the PDMS counterpart (thermal conductivity:  $0.193 \text{ W m}^{-1} \text{ K}^{-1}$ ). Numerous other opportunities exist, for instance, a microstructured ceramic infrared reflector (**Figure S6**, Supporting Information).

In summary, we describe a mechano-plastic pyrolysis process for creating 3D ceramics with complex hierarchical structural features spanning from macroscopic to submicron scales. This process uniquely explores the solid-state plasticity from the dynamic bond exchangeability of PDMS preceramic precursor. Rational choice of the catalyst permits seamless integration of the plasticity with the ability of pyrolysis. Besides the multiscale geometric control, consecutive plastic deformation and pyrolysis allow unparalleled freedom to manipulate microscopic features. The MPP process opens up many opportunities to fabricate high temperature resistant ceramic products/devices.

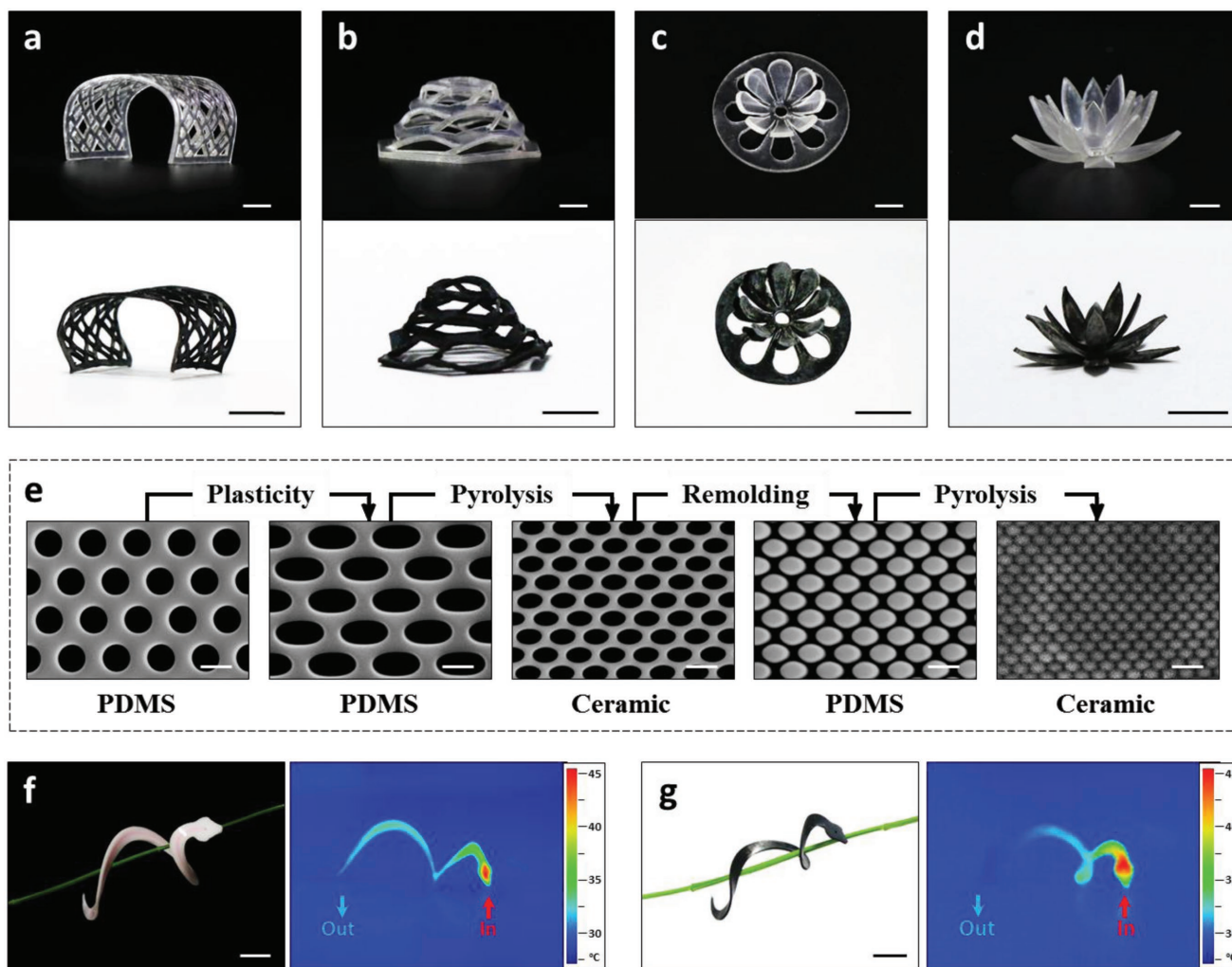


**Figure 4.** Micro- and macro-demonstrations of preceramic polymer and MPP ceramic. a–d) 3D preceramic polymer after plastic deformation (top) and the corresponding ceramics (bottom): laser-cut PDMS sheets (a–c); a multilayer structure obtained via interfacial self-bonding (d) (scale bar: 1 cm). e) Cyclic microstructure manipulation via plasticity, pyrolysis, and remolding (scale bar: 2  $\mu\text{m}$ ). f) Microfluidic device of PDMS nanocomposite (10% aluminium oxide). g) Microfluidic ceramic device. In (f,g), the colored photos represent the infrared images showing the temperature scale when hot water was injected (scale bar: 1 cm).

## Supporting Information

Supporting Information is available from the Wiley Online Library or from the author.

## Acknowledgements

The authors thank the following programs for the financial support: National Key Basic Research Program of China (Grant No. 2015CB351903); National Natural Science Funds for Distinguished Young Scholar (Grant No. 21625402); National Natural Science Foundation of China (Grant Nos. 21474084, 21474090, and 51673169). T.X. conceived the concept and wrote the paper. N.Z. designed the experiments. N.Z. and J.H. conducted the experiments. H.Z. fabricated the infrared reflector and performed the mechanical simulation. T.X. and Q.Z. supervised the project. All authors contributed to the discussion. N.Z. and J.H. contributed equally to this work.

## Conflict of Interest

The authors declare no conflict of interest.

## Keywords

ceramics, dynamic covalent polymers, plasticity, siloxane equilibration

Received: November 12, 2018

Revised: December 9, 2018

Published online:

- [1] E. Peng, D. Zhang, J. Ding, *Adv. Mater.* **2018**, *30*, 1802404.
- [2] R. F. Shepherd, P. Panda, Z. Bao, K. H. Sandhage, T. A. Hatton, J. A. Lewis, P. S. Doyle, *Adv. Mater.* **2008**, *20*, 4734.

- [3] Y. Xu, M. Guron, X. Zhu, L. G. Sneddon, S. Yang, *Chem. Mater.* **2010**, *22*, 5957.
- [4] R. Zauner, *Microelectron. Eng.* **2006**, *83*, 1442.
- [5] E. Medvedovski, M. Peltsman, *Adv. Appl. Ceram.* **2012**, *111*, 333.
- [6] A. Zocca, P. Colombo, C. M. Gomes, J. Günster, *J. Am. Ceram. Soc.* **2015**, *98*, 1983.
- [7] P. Colombo, G. Mera, R. Riedel, G. D. Sorarù, *J. Am. Ceram. Soc.* **2010**, *93*, 1805.
- [8] M. Peuckert, T. Vaahs, M. Brück, *Adv. Mater.* **1990**, *2*, 398.
- [9] *Polymer Derived Ceramics: From Nanostructure to Applications*, (Eds: P. Colombo, R. Riedel, G. D. Sorarù, H. J. Kleebe), DEStech, Lancaster, PA **2010**.
- [10] X. Liu, Y-L. Li, F. Hou, *J. Am. Ceram. Soc.* **2009**, *92*, 49.
- [11] Z. C. Eckel, C. Zhou, J. H. Martin, A. J. Jacobsen, W. B. Carter, T. A. Schaedler, *Science* **2016**, *351*, 58.
- [12] E. Zanchetta, M. Cattaldo, G. Franchin, M. Schwentenwein, J. Homa, G. Brusatin, P. Colombo, *Adv. Mater.* **2016**, *28*, 370.
- [13] A. A. Pawar, S. Halivni, N. Waiskopf, Y. B. Shahar, M. S. Harari, S. Bergbreiter, U. Banin, S. Magdassi, *Nano Lett.* **2017**, *17*, 4497.
- [14] J. Xing, M. Zheng, X. Duan, *Chem. Soc. Rev.* **2015**, *44*, 5031.
- [15] F. L. Bargardi, H. Le Ferrand, R. Libanori, A. R. Studart, *Nat. Commun.* **2016**, *7*, 13912.
- [16] G. Liu, Y. Zhao, G. Wu, J. Lu, *Sci. Adv.* **2018**, *4*, eaat0641.
- [17] W. Zou, J. Dong, Y. Luo, Q. Zhao, T. Xie, *Adv. Mater.* **2017**, *29*, 1606100.
- [18] Q. Zhao, W. Zou, Y. Luo, T. Xie, *Sci. Adv.* **2016**, *2*, e1501297.
- [19] N. Zheng, Z. Fang, W. Zou, Q. Zhao, T. Xie, *Angew. Chem., Int. Ed.* **2016**, *55*, 11421.
- [20] S. Billiet, K. De Bruycker, F. Driessen, H. Goossens, V. Van Speybroeck, J. M. Winne, F. E. Du Prez, *Nat. Chem.* **2014**, *6*, 815.
- [21] G. Zhang, Q. Zhao, L. Yang, W. Zou, X. Xi, T. Xie, *ACS Macro Lett.* **2016**, *5*, 805.
- [22] T. F. Scott, A. D. Schneider, W. D. Cook, C. N. Bowman, *Science* **2005**, *308*, 1615.
- [23] B. T. Michal, C. A. Jaye, E. J. Spencer, S. J. Rowan, *ACS Macro Lett.* **2013**, *2*, 694.
- [24] D. Montarnal, M. Capelot, F. Tournilhac, L. Leibler, *Science* **2011**, *334*, 965.
- [25] D. J. Fortman, J. P. Brutman, C. J. Cramer, M. A. Hillmyer, W. R. Dichtel, *J. Am. Chem. Soc.* **2015**, *137*, 14019.
- [26] K. Jin, L. Li, J. M. Torkelson, *Adv. Mater.* **2016**, *28*, 6746.
- [27] P. Zheng, T. J. McCarthy, *J. Am. Chem. Soc.* **2012**, *134*, 2024.
- [28] W. Schmolke, N. Perner, S. Seiffert, *Macromolecules* **2015**, *48*, 8781.
- [29] K. L. Ngai, C. M. Roland, *Macromolecules* **1993**, *26*, 2688.
- [30] F. Meng, R. H. Pritchard, E. M. Terentjev, *Macromolecules* **2016**, *49*, 2843.